



Cortical networks of the mouse brain elaborate within the gray matter

Akiya Watakabe¹ · Junya Hirokawa²

Received: 15 February 2018 / Accepted: 3 July 2018
© Springer-Verlag GmbH Germany, part of Springer Nature 2018

Abstract

In primates, proximal cortical areas are interconnected via within-cortex “intrinsic” pathway, whereas distant areas are connected via “extrinsic” white matter pathway. To date, such distinction has not been clearly done for small-brained mammals like rodents. In this study, we systematically analyzed the data of Allen Mouse Brain Connectivity Atlas to answer this question and found that the ipsilateral cortical connections in mice are almost exclusively contained within the gray matter, although we observed exceptions for projections from the retrosplenial area and the medial/orbital frontal areas. By analyzing axonal projections within the gray matter using Cortical Box method, which enabled us to investigate the layer patterns across different cortical areas, we obtained the following results. First, widespread axonal projections were observed in both upper and lower layers in the vicinity of injections, whereas highly specific “point-to-point” projections were observed toward remote areas. Second, such long-range projections were predominantly aligned in the anteromedial–posterolateral direction. Third, in the majority of these projections, the connecting axons traveled through layer 6. Finally, the projections from the primary and higher order areas to distant targets preferentially terminated in the middle and superficial layers, respectively, suggesting hierarchical connections similar to those of primates. Overall, our study demonstrated conspicuous differences in gray/white matter segregation of axonal projections between rodents and primates, despite certain similarities in the hierarchical cortical organization.

Keywords AAV · Anterograde tracers · Cortico-cortical projection · Feedforward · Feedback · White matter

Introduction

Expansion of the cerebral cortex and its differentiation into many specialized areas is one of the most distinguished features of the mammalian brain evolution. The connections among these cortical areas lay the basis for the functional integrity of the cortex as a whole. In macaques and other non-human primates, anterograde tracer experiments found

two modes of cortical connections: the distant areas are connected via bundles of axons that travel through the white matter (“extrinsic” connection), whereas the nearby areas are connected via “intrinsic” or “horizontal” cortical connections that are contained entirely within the gray matter (Levitt et al. 1993; Lund et al. 1993). How, then, are cortical areas connected in small-brained animals like mice? Although much smaller in size, the mouse cortex also has complex cortical organization (Horvát et al. 2016; Goulas et al. 2017). The visual system, for example, has multiple higher visual areas that each has unique inter-areal connectivity (Wang and Burkhalter 2007; Wang et al. 2012). It is possible that they are interconnected via the white matter as in primates. On the other hand, the whole mouse cortex is much smaller than macaque V1 (Finlay 2016). In terms of size, the mouse cortex may exhibit intrinsic-type connectivity.

As expected from its importance as a model animal for neuroscience studies, there have been many efforts to elucidate the cortical connectivities in rodents (e.g., Schüz et al. 2006; Oh et al. 2014; Paxinos 2014; Zingg et al. 2014;

Akiya Watakabe and Junya Hirokawa contributed equally to this work.

Electronic supplementary material The online version of this article (<https://doi.org/10.1007/s00429-018-1710-5>) contains supplementary material, which is available to authorized users.

✉ Akiya Watakabe
akiya.watakabe@riken.jp

¹ Riken, Center for Brain Science, 2-1 Hirosawa, Wako, Saitama 351-0198, Japan

² Laboratory of Neural Information, Doshisha University, 1-3 Tatara Miyakodani, Kyotanabe, Kyoto 610-0394, Japan

Horvát et al. 2016; Gămănuț et al. 2018). However, there has been little mention in the literature on where axonal fibers actually pass through. In a classic single cell tracking study, Dechenes et al. showed several examples of rat S1 neurons projecting to S2 via the gray matter (Zhang and Deschêes 1997). Likewise, we labeled the callosally projecting M1 neurons by double viral strategy and found their collateral projections to reach the ipsilateral S1 via the gray matter (Watakabe et al. 2014). These observations raise the possibility of gray matter pathway for mouse cortical connections but they are too fragmental to generalize: other cell types may project to distant targets via the white matter even in S1 or M1 and/or there may exist white matter connectivity between other areas. To clarify this point, there is a need for systematic analyses of the route of axonal projections in rodents.

In this article, we approached this question using a publicly available database of Allen Institute for Brain Science (<http://connectivity.brain-map.org/>). In this database, there exist serial image data of hundreds of samples, in which AAV-based anterograde tracers were injected at a single site per mouse. By detailed examination of their dataset, here we show that most of the long-range corticocortical projection within the ipsilateral hemisphere travel through the gray matter. We also quantitated layer-specific distribution of the axonal signals by modified Cortical Box method, which is a kind of a flat map with laminar information (Hirokawa et al. 2008a, b; Watakabe et al. 2012). Combined with clustering analysis, it provided an objective means to investigate the complex architecture of axonal projections within the gray matter. By these analyses, we found evidence for similar hierarchical relationships among cortical areas as suggested previously for the visual areas (Coogan and Burkhalter 1993; D'Souza et al. 2016; D'Souza and Burkhalter 2017). Thus, our study highlighted the similarity and difference of cortical wiring between rodents and primates, which provides insight to translational studies across species.

Materials and methods

Confocal microscopic analyses

For confocal microscopic imaging of the cortico-cortical fibers, we used the brain sections from our previous study (Watakabe et al. 2014). Specifically, we used the section of mouse #456, in which NeuRet vector encoding TRE-SYP_CFP was injected into S1 and AAV encoding Syn-rtTAV16 was injected into M1. The sections were pretreated with 80% methanol/20% dimethyl sulfoxide solution (Dent's solution) and immunostained with the anti-GFP antibody (1:20,000, Tamamaki et al. 2003) followed by Cy2 conjugated anti-rabbit IgG 1:1000, as described previously (Watakabe et al.

2014). After mounting on a slideglass, the stained sections were imaged by Olympus Fluoview FV1000 confocal microscopy using 40X water immersion lens.

Digital data acquisitions

We downloaded a series of dataset from a public database of mouse connectome at <http://www.alleninstitute.org> (Allen Mouse Brain Connectivity Atlas 2011). They conducted a brain-wide anterograde tracing with enhanced green fluorescent protein (EGFP)-expressing AAV in mice (Oh et al. 2014). Seventeen datasets shown in Table 1 were selected for detailed analyses, which include areas with various functions and topological positions. We used only the wild-type mice, because we wanted to examine all the potential projections from the area of interest. The XY resolution of the original dataset was 0.35 $\mu\text{m}/\text{pixel}$ and the imaging was performed with 100 μm intervals in Z direction. For high magnification views, we used the original resolution images. For other purposes, including Cortical Box analysis, we downloaded 1/8 compressed version of 8bit RGB, JPEG format images without changing the default contrast for each image.

Standardization of regions of cortex

The cortical box method was performed as previously described (Hirokawa et al. 2008a, b; Watakabe et al. 2012). The method compresses a coronal cortical section into a standardized 2D matrix aligned to cortical layers and assembles the 2D matrices from serial sections into a standardized 3D box. Because the matrix data is formatted for quantitative analysis of cortical layers, the method enables us to capture layer patterns buried in the whole brain data across animals by analyses such as virtual slices and clustering. Region of interests (ROIs) in the cortical sections were defined manually based on structural landmarks as follows. The medial end of the white matter and the valley of the rhinal fissure were chosen as structural landmarks of the mediodorsal (MD) and lateroventral (LV) ends of the cortical sections, respectively. The border between the cortex and the white matter were carefully chosen based on the presence/absence of cell bodies, as shown in Fig. 1i–k. The pial surface and the bottom of the white matter area was used as the outer (OC) and the inner contours (IC), respectively. Then, our customized program automatically divided the cortical part into columns. The lengths of OC and IC were equally divided into 101 points resulting 100 segments defined by every two adjacent points on each contour. Each division (i.e., column) was standardized by linear interpolation (130×10 pixels, depth and width, respectively) and these divisions from MD to LV were aligned from left to right, which became the “standardized cortical section” (130×1000 pixels, depth and width, respectively). The relative intensities of the tracer

Table 1 Analyzed areas in the present study

ID	Classification	Injection area		Allen data ID	
		Primary	Secondary		
Motor					
1	<Primary>	MOp (62%)	Primary motor area	SSp-ul (38%)	126909424
2		MOp (59%)	Primary motor area	SSp-ll (36%)	180720175
3	<Higher>	MOs (62%)	Secondary motor area	ACAd (38%)	141603190
4		MOs (96%)	Secondary motor area	–	180916954
Somatosensory					
5	<Primary>	SSp-m (100%)	Primary somatosensory area, mouth	–	114290938
6		SSp-n (100%)	Primary somatosensory area, nose	–	126908007
7		SSp-ll (50%)	Primary somatosensory area, lower limb	SSp-ul (49%)	112791318
8		SSp-tr (57%)	Primary somatosensory area, trunk	SSp-ll (19%)	126852363
9		SSp-bfd(83%)	Primary somatosensory area, barrel field	–	126907302
10	<Higher>	SS-s (99%)	Secondary somatosensory area	–	117298988
11		SS-s (n.a.)	Secondary somatosensory area	–	113036264
Auditory					
12	<Primary>	AUDp (56%)	Primary auditory area	AUDpo (43%)	146858006
13	<Higher>	AUDd (67%)	Dorsal auditory area	AUDp (18%)	158314278
Visual					
14	<Primary>	VISp (53%)	Primary visual area	VISl (43%)	309004492
15	<Higher>	VISa/am(67%)	Anterior and anteromedial visual area	VISa (33%)	126861679
Medial association					
16		ACAd (67%)	Anterior cingulate area	ACAv (33%)	139426984
17		RSPv (93%)	Retrosplenial area, ventral part	–	100148142
Frontal pole					
18		MOs (81%)	Secondary motor area	AId(17%)	180719293
19		PL (56%)	Prelimbic area	IL(32%)	157711748
20		AId + AIv (63%)	Agranular insular area	ORB1 (33%)	180709230
21		ORB1 (83%)	Orbital area	ORBvl (16%)	112306316
22		ORBvl (76%)	Orbital area	PL (9%)	112423392
23		AId (83%)	Orbital area	MOp (15%)	112596790

Primary and secondary injection area indicates spread of AAV virus to multiple areas upon single injections

signals were normalized by the maximum and used for subsequent analyses. In Fig. 6, we extended the analysis to the area around the medial wall. The bottom of the medial wall and the symmetric counterpart in the cortex were manually chosen as the medial (ME) and lateral (LE) ends. Note that we only used the medial box method to visualize individual projections without comparing across samples, since the method does not allow objective definition of the ROI. To reduce the effort to make cortical box from sections without signals, we used 21–57 coronal sections in each projection so that we can cover the injection site and the major projections in each projection.

To allow comparison of the cortical boxes between different samples, we aligned the anterior–posterior positions based on the shape of the hippocampus in reference to

the Paxinos and Franklin (2004). We limited the analysis in the range between Bregma distance of + 1.5 to – 4.6, spanning from primary visual cortex to motor cortex with a resolution of 100 μ m. Therefore, a standard cortical box consists of three-dimensional data; 61 \times 1000 \times (100 + 30) data points [AP length \times ML width \times (layer depth and white matter fraction)] with the relative intensities of fluorescent signals expressed with percentages (0–100%). To generate the standardized map of a particular layer, the specific layer fraction (1–10% for layer 1; 75–100% for layer 6) and white matter fraction were extracted from the standardized cortical box and compressed into a two-dimensional map by averaging the fraction with a Gaussian filtering using a kernel of 7 pixels. Visualizations were carried out using Matlab 2017 (Mathworks, Natick, MA,

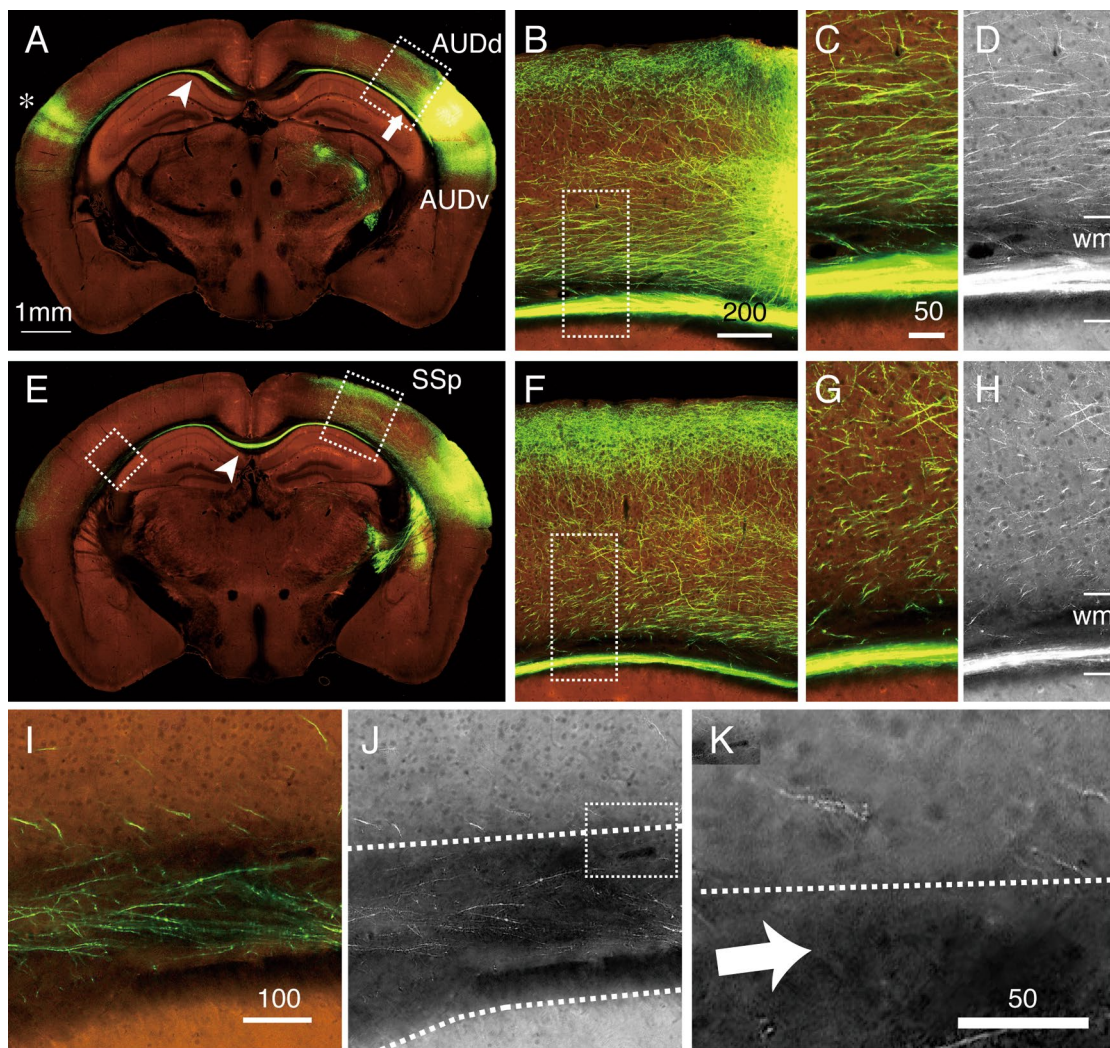


Fig. 1 Image data from Allen Mouse Brain Connectivity Atlas analyzed for the axonal projections. The AAV tracer was injected into AUDd (Table 1: ID13) and the axonal spread of GFP signals were imaged by Serial two-photon tomography. **a** The coronal plane with the center of injection. The white arrow indicates the axon bundle within the white matter that projects towards the contralateral area (shown by asterisk). Note that the intensity of the fluorescence does not change much when compared between the intensity right after entering the white matter (arrow) and after entering the contralateral hemisphere (arrowhead). The dotted box is magnified in **b**. Bar 1 mm. **b** The magnified view of axons projecting from the injection site. Note that, few, if any, axon fibers exist between the white matter bundle and the fibers in the bottom of layer 6. The dotted box is magnified in **c**. Bar: 200 μm. **c** Magnified view around the border between layer 6 and the white matter. Bar 50 μm. **d** Red channel view of the image shown in **c**. This channel shows the autofluorescence background of the tissues with some leak of green tracer signals. The border between the white matter (wm) and layer 6 was determined

by darkness of white matter and the cell shadows (see “Materials and methods”). **e** The coronal section view, which is anterior to that in **a**. The arrowhead indicates the axon fibers crossing the corpus callosum. Note the axonal projections to upper layers in SSp. Magnification is the same as in **a**. **f** Magnified view of the dotted box around SSp of **e**. Magnification is the same as in **b**. **g** Magnified view of the dotted box of **f**. Magnification is the same as in **c**. **h** Red channel view of the image shown in **g**. **i** Magnified view of the dotted box in the contralateral hemisphere of **e**. Note the presence of axon fibers within the white matter. Bar 100 μm. **j** Red channel view of the image shown in **i**. **k** Magnified view of the dotted box in **j**. The dotted line shows the border between layer 6 and the white matter. Note the presence of cell shadows in layer 6. The border is determined by the overall autofluorescence intensity. So, the presumptive white matter region may include some “layer 6”, because we can see very weak cell shadows (white arrow). In order not to underestimate the “white matter”, we prioritized the overall fluorescence intensity over cell shadows in border determination

USA). Note that the assignment of the layers in the cortical box analysis is approximate except for the white/gray matter border because it was uniformly done regardless

of areas. In our previous studies, it still proved to be quite effective (Hirokawa et al. 2008a).

Annotation of cortical areas

To annotate the cortical areas, we relied on the annotation by the Allen Mouse Brain Connectivity Atlas. This database provides two ways to annotate cortical areas. First, in their “cortical map signal viewer”, they provide flatmap version of the cortical signals with annotation. We were able to identify the region with concentrated tracer signals by comparing their map with coronal images and with our Cortical Box views. Second, their atlas is coupled with the Nissl-based reference atlas. We annotated the cortical areas based on such information. Thus, the nomenclature of the areas in our study is in accordance with that of the Allen atlas, except for Fig. 9, in which S1 for the somatosensory cortex and M1 for the motor cortex were used.

Data analysis of standardized cortical map

For clustering analysis, 17 injection samples were analyzed (Table 1). White matter fraction was removed from the cortical box data for this purpose. Each of the cortical boxes was compressed by downsampling the ML width from 1000 points to 100 point with nearest neighbor method to reduce the computational burden, resulting in a reduced cortical box ($61 \times 100 \times 100$, AP length \times ML width \times layer depth). The 3D matrix for each injection sample was then converted to 2D, keeping the depth information (6100×100 ; location \times layer depth). The columns in the matrix (corresponding to cortical columns) with low signals (mean intensity less than 50) were removed from the matrix as a background noise. The rest of the columns from 17 cortical boxes were combined into a single matrix as a $P \times N$ matrix (row \times column), where P is the location number ($P = 24,000$), and N is the number of cortical layer data ($N = 100$). Each column of this matrix was normalized using the maximum and minimum of the data in that column. The data matrix was subjected to hierarchical cluster analysis using Ward’s algorithm. To determine the optimal number of the clusters, clustering was conducted by systematically changing cluster number and the variance from the average was calculated for each cluster and summated to calculate “total within sum of square”, which provided the measure of similarities within the cluster (Fig. 8A). Based on this evaluation, we set the cluster number to five and performed the subsequent analyses.

To test the robustness of the result of clustering against samples used, we performed clustering using a subset of the 17 injection samples and calculated the similarity of thus-obtained patterns with the original patterns. In more detail, we randomly chose a subset ($N = 1-16$) of the 17 samples and performed the clustering analysis with a fixed cluster number ($n = 5$). Each clustering analysis generated five averaged layer patterns and they were compared with the original

five patterns (Fig. 8B) for the best matching. Then, the Pearson’s correlation coefficient was calculated between the new and the original patterns and five of them were averaged as the similarity value of the new clustering as a whole. We repeated 20 times of random sampling for each sample number ($N = 1-16$) and the average of the 20 similarity values were plotted against the sample number (shown in red in Online Resource 3). For comparison, we also calculated the correlation coefficients among the five patterns generated for each clustering and the highest values were averaged for each sample number (shown in blue in Online Resource 3). To exclude a possibility that the clustering results are confounded by the heterogeneity of the injection areas, only samples with relatively restricted injection site ($> 96\%$) were selected (ID 4, 5, 6, 7, 10, 16, 17 in Table 2) instead of all the 17 samples and repeat the same analysis above (shown in green in Online Resource 3). Online Resource. 3, thus, also indicates that the similarity across the clusters is low, even if the sample numbers are reduced.

To visualize the spatial distributions of thus-classified columnar lamina patterns, each point on the flatmap was color-coded for five patterns and remapped on the layer map for each injection. Overlaid on this color-coded map was the maximum intensity projection of all layers (shown as

Table 2 Laminar preference of innervation at remote targets

ID	Area	Two farthest targets			
<primary areas>					
1	MOp	SS-s	b	SS-s	b
2	MOp	SS-s	b	AUDd	c
5	SSp-m	SS-s	a	VISC/TEa	b
6	SSp-n	MOp	b	VISC/TEa	b
7	SSp-ll	SS-s	b	AUDp	c
8	SSp-tr	AUDv	b	AUDd	b
9	SSp-bfd	MOs	a	AUDd	b
12	AUDp	AUDv	b	VISp	a
14	VISp	VISa/am	a	VISrl	b
		b (%)	66.7	a + d (%)	22.3
<higher order areas>					
3	MOs	SSp	d	VISrl	d
4	MOs	VISam	d	VISrl	d
10	SS-s	MOp	b	SSp	e
11	SS-s	MOp	a	MOs	a
13	AUDd	SSp	a	SS-s	a
15	VISa/am	SS-s	d	VISa/am	
16	ACAd	VISa/am	a	RSPd	d
17	RSPv	RSPv	d	VISrl	d
		b (%)	6.3	a + d (%)	87.5

FFI (feedforward index) = $b/(a + d)$

FFI = 2.74 for primary areas; FFI = 0.072 for higher order areas (bootstrap, $p = 0.000226$)

contours in Online Resource 1). This MIP map was used to identify the target areas, which exhibit locally high values at locations distant from the injection site, as well as to manually track the local maximums from the injection site to such target areas. For cross-sample analyses, we selected two furthest target areas for pathway analysis for remapping on a common coordinate (see above) (Fig. 8E, Online Resource 2). We consider that the selection of the furthest target areas is the most unbiased way for analysis of the long-range projections. The lamina patterns at the same target areas were also used to analyze differential preferences of the projections from the primary and higher-order areas (see below). Although the tracer signals in the current study include both the synapsing and passing fibers, we expected that the lamina patterns at the peripheral targets should reflect the synaptic connections better, whereas the projections to the nearby sites may contain passing fibers with no boutons.

To evaluate the difference of the target layer patterns for the projections from the primary and higher-order areas, we calculated the feedforward index ($b/(a+d)$), which compare the middle-layer dominant projections to superficial layer dominant projections. The significance of the difference of the feedforward indices between the primary and the higher order areas was validated by bootstrap method (10,000 repetitions) by re-assigning primary and higher order areas pseudo-randomly.

Data and statistical analyses

The primary data of Serial Two-photon tomography was obtained from Allen Mouse Connectivity atlas (<http://www.alleninstitute.org>). The datasets generated during and/or analyzed during the current study are available from the corresponding author on reasonable request. The statistical significance of the bias in the direction for long-range projections was determined by Kuiper test. The statistical significance of differential pattern distribution for the primary and higher-order areas was tested by bootstrap method (Table 2; see above). Student's *t* tests were performed for comparison of the pattern distribution for the primary and higher-order areas in Online Resource 3A. Matlab was used for calculation and all values are expressed as means \pm SEM.

Results

Examination of AAV-based anterograde tracers of Allen Mouse Brain Connectivity Atlas

Allen Mouse Brain Connectivity Atlas (<http://connectivity.brain-map.org/>) provides hundreds of serial image data for anterograde tracer injections for wild type and transgenic lines. Among the dataset, we selected only those using the wild type

mice and AAV with synapsin-promoter driven EGFP. This AAV tracer works as an efficient anterograde tracer and labels cell bodies, dendrites, axonal fibers and terminals efficiently. The sections are imaged by serial two-photon tomography with 100 μ m interval (Ragan et al. 2012; Oh et al. 2014). We browsed through the dataset and selected 17 injections for detailed analyses and 6 injections in the frontal pole regions for visual inspection (Table 1) among 128 candidate injections. These injections were selected based on (1) high level of labeling, (2) high quality of imaging and (3) variety of cortical areas to represent both primary and higher order areas from the motor, somatosensory, auditory and visual systems.

Figure 1 shows an example of injection into the dorsal auditory area (AUDd). In this example, there was a robust projection dorsally to the somatosensory cortex (Fig. 1e, SSp). At first sight, the thick axon bundle just beneath the innervation target appears to provide the axonal projections. At high magnification, however, we could rarely observe branching of fibers out of this bundle into the gray matter (Fig. 1c, g). This axon bundle proceeded through the corpus callosum without losing fluorescent intensity (Fig. 1a, e, arrowheads) and innervated the contralateral side (Fig. 1a; asterisks, Fig. 1i). On the other hand, the axon fibers that projected out medially from the injection site (Fig. 1b) continued across sections toward the AP-level of SSp (Fig. 1f). In particular, relatively thick fibers populated within layer 6 to reach the bottom part of SSp, where they branched into thinner fibers, turned perpendicular to the layers and innervated layers 1–3 (Fig. 1f). These observations suggest that the projection from AUDd to SSp occurs through widespread axon fibers that are contained within the gray matter. The axons from AUDd also projected ventrally to innervate AUDv (Fig. 1a). This adjacent projection occurred in a side-by-side manner within the gray matter, which is reminiscent of intrinsic connections as is observed with the primate brains.

One key point of observation for the above conclusion is the distinction between the white matter and the gray matter. In this and the subsequent studies, we drew borders based on the intensity of the tissue autofluorescence in the red channel (Fig. 1i–k). With this criterion, the “bright” region is definitely a gray matter, because the shadows of cell bodies observed at high magnification tell us that the region is densely populated with neuronal cells. The “dark” region may include some “gray matter”, but we classify such region as “white matter” in order not to underestimate the white matter region.

“Gray matter route” is a rule rather than an exception for cortico-cortical connections

To confirm the generality of the observations of AUDd injection, we examined other cortical projections. Figure 2

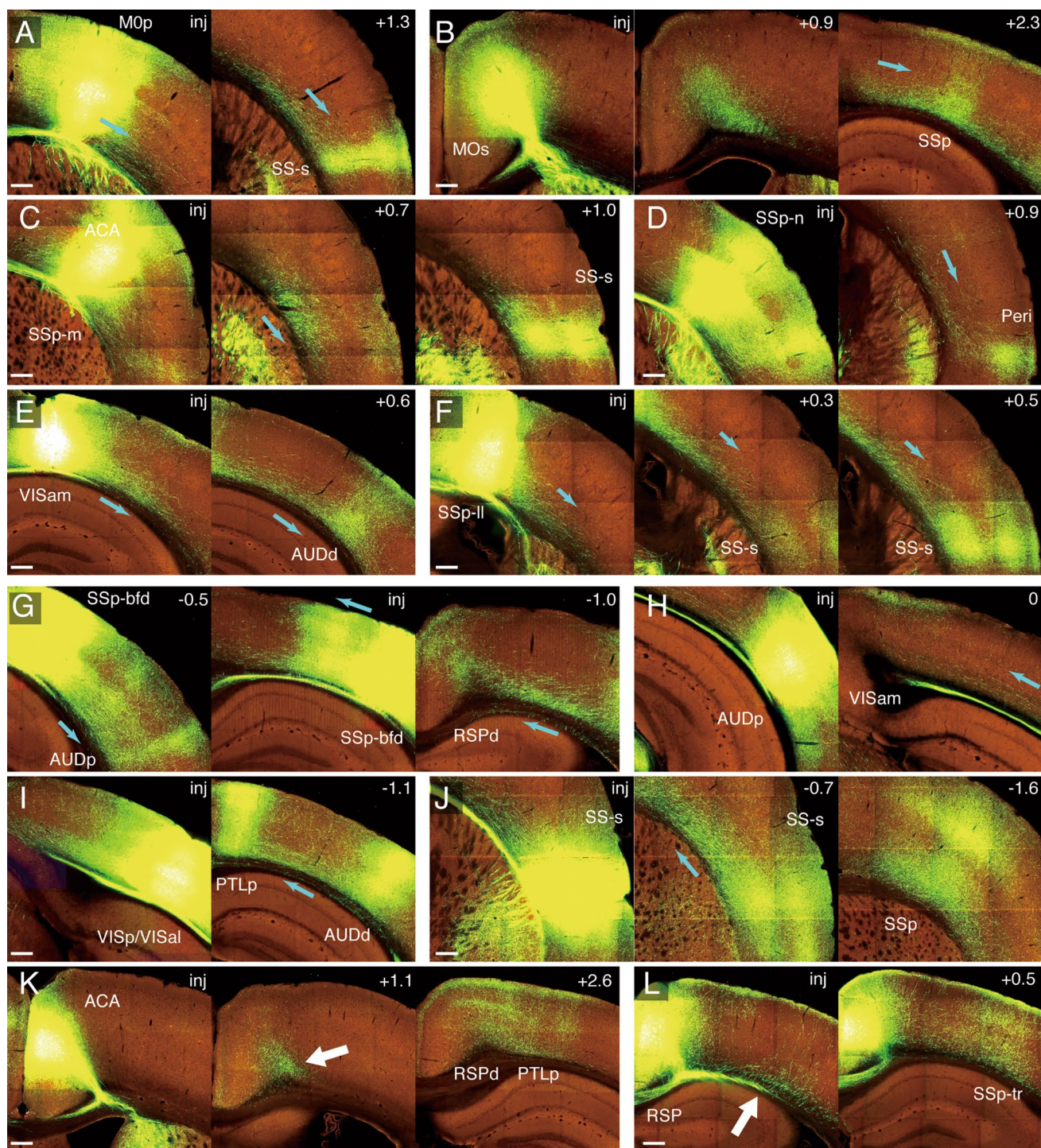


Fig. 2 Example images of Allen Mouse Connectivity atlas dataset showing “gray matter route” of various cortico-cortical projections. **a–l** A set of images showing the gray matter route of projections from the injection site to one of the projection targets. The direction of axonal flows is shown by cyan arrows in each panel judged by the angle of axon fibers and relative positions. The number on the top right indicates the section positions of the image in reference to

the injection site (inj) in mm (the number increases to the posterior direction). The areas of injection and targets were judged as in “[Materials and methods](#)”. The Allen data ID for these images are as follows (also see [Table 1](#)): **a** 126909424; **b** 141603190; **c** 114290938; **d** 126908007; **e** 126861679; **f** 112791318; **g** 126907302; **h** 146858006; **i** 309004492; **j** 117298988; **k** 139426984; **l** 100148142. Bar 250 μ m

illustrates 12 typical cases of cortical projection patterns (Cyan arrows indicate the overall direction of the axon tracts). Figure 2a–f exhibit the cases in which axons projected toward the areas on the lateral side. In all these cases, we observed axon fibers that travel through layer 6 toward the target area, where they turned oblique to the laminar planes and terminated in a columnar fashion. The thick axon bundles that entered the white matter either turned medially to project to the contralateral cortex or entered into the internal capsule. In some instances, we observed relatively thin axon fibers to go through the white matter ventrolaterally (e.g., Fig. 2f). In such cases, axon fibers appeared to enter the striatum but not the cortical gray matter (e.g., Fig. 3e, lower arrow). Figure 2g–j represent examples of medial projections. Similar to the injection to AUDd (Fig. 1), the thick axon fibers within the white matter were callosally projected and the innervation of the ipsilateral cortical areas occurred within the gray matter, especially within layer 6. Figure 2k, l represent two cases, in which AAV tracer was injected to the medial wall of the cortex. Whereas the injection into ACA resulted in a similar layer 6 routing as other areas (Fig. 2k), the projection from RSP toward SSp-tr branched off from the thick axon bundle in the white matter that connected to the internal capsule (Fig. 2l). So, this is a rare exception to take “white matter route” to reach the distant target in the ipsilateral cortex.

To see if the axon fibers from the higher-order association areas in the frontal pole region take the gray or white matter route, we inspected the projection patterns for secondary motor area (MOs), prelimbic area (PL), agranular insular area (AI), and orbitofrontal areas (ORB). First, despite at rostral location, the projections from the MOs exhibited essentially the same profile as those for posterior MOs. That is, direct innervation was sparse in the white matter for the ipsilateral projections, in contrast to extensive white matter innervation for the contralateral projections (Online Resource 5, panels A4 and A5). Second, the projections from PL, AI and ORB to the dorsal and/or lateral cortices initially crossed the white matter just anterior of the head of the caudate-putamen to take the shortest pathway to reach the other side (e.g., Online Resource 5, panels B3, C3 and D3). Furthermore, for dorsal projections from ORB, we observed some axon fibers to extend within the white matter to reach MOp (Online Resource 5, panels D4 and E4). These observations suggest that at least a part of the cortical projections take the white matter route to innervate the caudal areas. However, such white matter signals were not present below SSp and SSs. For these areas, the axon fibers likely proceeded through MOp and/or MOs gray matter (Online Resource 5, panels D4, D6, E4–E6, E4/E5). Finally, the axon fibers for the lateral projections generally proceeded within the gray matter once they entered the claustrum and/or the insular cortex (Online Resource 5, panels B4–B6, C4–C6,

E4/E5, F4/F5). We conclude that the axon fibers from the frontal cortices can also take the gray matter route to remote targets, although a part of it may initially proceed within the white matter.

Visualization of cortical connections by Cortical Box method

To precisely follow trajectory of axon fibers, it is necessary to analyze the continuity of axonal signals across many section images. For this purpose, we employed Cortical Box method that we previously devised to characterize laminar and area architecture of rat cortices (Hirokawa et al. 2008a, b; Watakabe et al. 2012). In this method, a strip of dorso-lateral cortical areas is first segmented out of the original image for transformation (Fig. 3A). At this point, the white and gray matter is manually distinguished with the presence of neuronal cell body “shadows” as the criteria for the gray matter (see Fig. 1i–k). This strip is converted to a rectangle and the series of the rectangles are converted to a box. By re-slicing this box at particular lamina positions, we can have layer-specific flatmaps for the spread of axonal fluorescent signals (Fig. 3C).

Figure 3 shows an example of Cortical Box representation of AAV tracer injection into SSp-II (Allen data ID112791318; see Table 1). In the original coronal section images (Fig. 3D, F, H), the axonal projections originating from the injection site (Fig. 3D) were observed to proceed posterolaterally within layer 6 to reach columns b (Fig. 3F) and c (Fig. 3H). We used 28 of such images (section #63–90) to reconstruct the Cortical Box and re-sliced them to present the flatmaps for layer 1, layer 6 and the white matter (Fig. 3J–L). These flatmap representations clearly displayed areal distribution of axonal signals. In both layer 1 and layer 6 maps, the dense distribution of the tracer signals in and around the injection site can be seen (Fig. 3J–L, circles inj). In layer 1 map, two conspicuous columnar projections described above were very well visualized as spots b and c (Fig. 3J; arrows b, c). In addition, two weak neighboring columns shown in Fig. 3H (denoted by arrow d) were also visualized as two weak spots in this flatmap. For all these spots, axon signals were present at the corresponding location in layer 6 flatmap (see arrows b–d) as well, suggesting that axons projected vertically from layer 6 to layer 1 (Fig. 3K). In layer 6 map, the tracer signals spread widely from the injection site to these spots to be connected with each other. In contrast, we did not observe such pathways between the injection site and spots b, c and d within the white matter (Fig. 3L).

In the white matter, very strong tracer signals were only present in positions that correspond to the axon fibers that proceed toward the corpus callosum (Figs. 3D, 4l; cc) and those toward the internal capsule (Figs. 3D, 4l; ic). We did

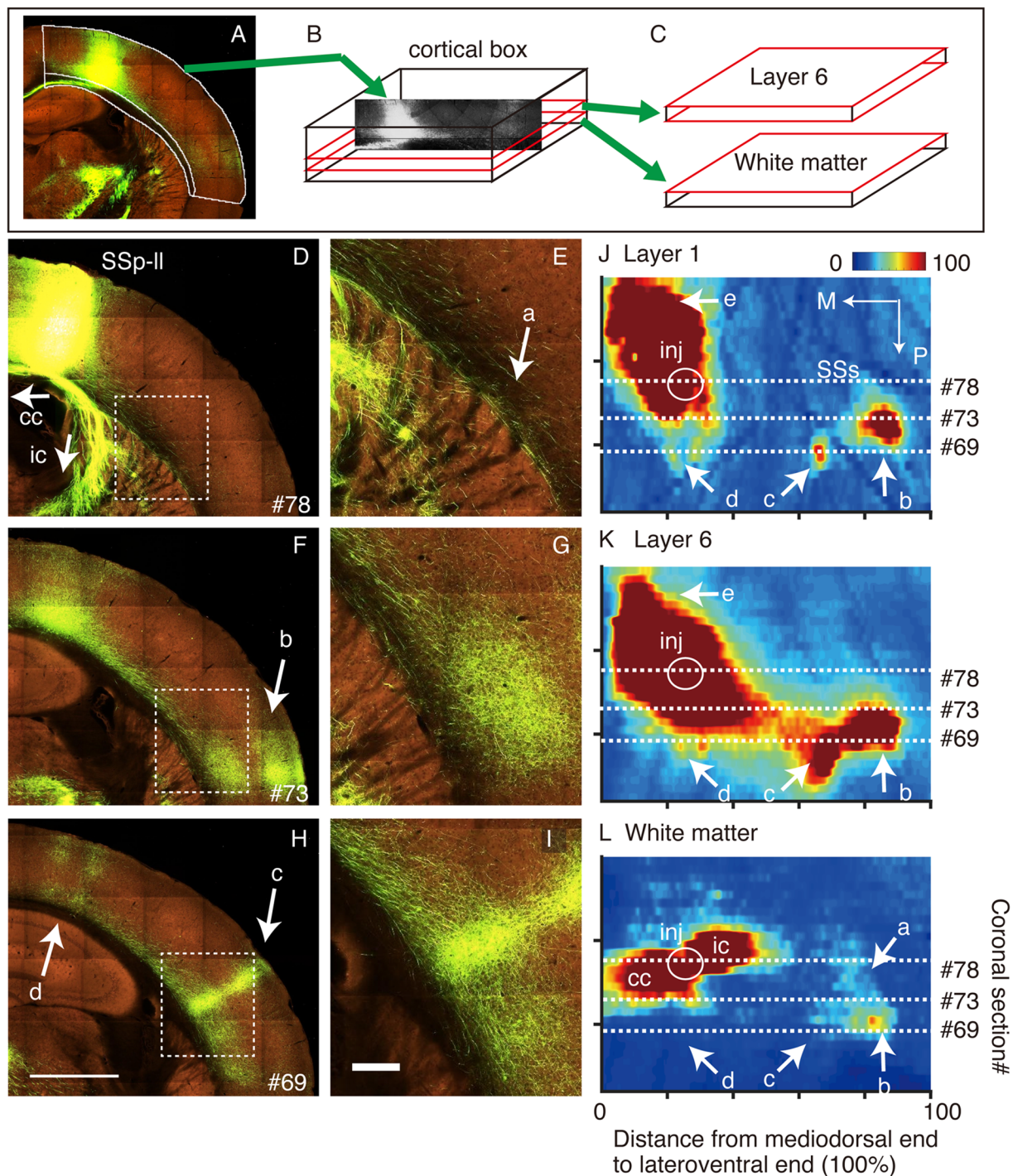


Fig. 3 Cortical Box representation of the axonal spread for SSp-II injection. **A–C** The schematic view of cortical box method. Example of a cortical section of SSp-II (Allen data ID112791318; see Table 1) targeted image (**A**). The mediodorsal end, lateroventral end, inner contour, and outer contour were manually determined to select the part of the cortex for further processing. The selected cortical region was converted into a standard rectangle (**B**). The same procedure was repeated for a set of coronal sections to reconstruct 3D image of the cortex (cortical box). A specific layer fractions (e.g., layer 6 and white matter) were extracted to demonstrate axonal spread in two-dimensional flatmaps (standardized layer maps). **D–L** Examples of the original coronal section images (**D, F, H**) and the magnified cor-

tical areas (**E, G, I**) indicated by dotted rectangles in the left panel were shown for comparison with the standardized layer maps for layer 1, 6 and white matter (**J–L**). The numbers in the right-bottom in **D, F, H** indicate the coronal section serial number from Allen Mouse Brain Connectivity atlas, of which corresponding positions were indicated in the standardized layer maps **J–L**. Injection site (inj) is determined by the extent of strong cell body labeling in the blue channel. The spots indicated by arrows **b–d** in flatmaps are columnar innervations that correspond to those in **F** and **H**. The weak signal in the white matter flatmap (**L**) indicated by arrow include corticostriatal fiber shown in **E**. Scale bars for **D, F, H**; 1 mm, for **E, G, I**: 200 μ m. *cc* corpus callosum, *ic* internal capsule

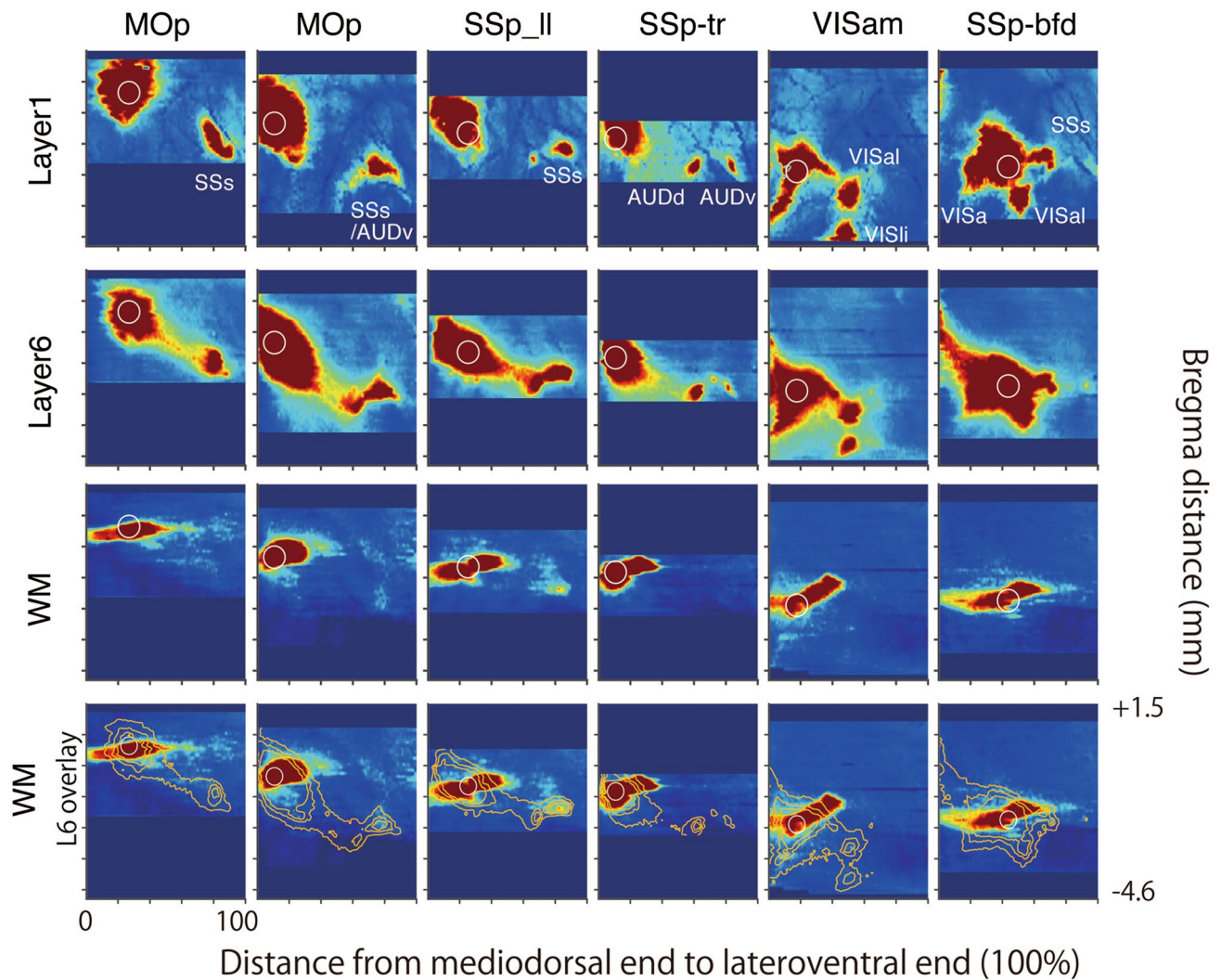


Fig. 4 Spatial distribution of axonal spread in standardized cortical flatmaps (1). Standardized layer flatmaps for 6 different AAV tracer injections. Layer 1, 6 and white matter flatmaps were shown as typical examples. To compare different projections in the same coordinate, the anterior–posterior positions of each dataset were identified based on anatomical landmarks in reference to the Paxinos and Franklin (2004) atlas (see “Materials and methods”). Although we

did not perform more precise registration, the Y position in each layer flatmap is considered to roughly correspond to the Bregma distance shown on the right. The dark blue space in the map indicates the area where we did not perform Cortical Box transformation. The white circles indicate the injection positions of AAV tracer. The bottom figures are the same as white matter map except that the contour of the signal from layer 6 map was overlaid as orange lines for comparison

observe some weak signals to continue from the internal capsule signals toward the lateral direction (see Fig. 3E, G). At least, a part of these signals come from the white matter fibers that enter the striatum (Fig. 3E, denoted by arrow a). Either way, comparison of layer 6 and white matter maps showed that the majority of cortical projections proceed within the gray matter.

Flatmap analyses demonstrate the predominance of “gray matter route” for cortical projections

In the present section, we examined the areal distribution patterns of tracer signals for 17 injections listed in Table 1

(also see Online Resource 2 for topological localization), using layer-specific flatmaps. This analysis provided overviews of different injections and reinforced our observation of the predominance of the gray matter route for cortical projections. In Fig. 4, AAV tracer was injected in the medial sides, whereas in Fig. 5, AAV tracer was injected in the lateral sides. Figure 6 presents four cases of medial wall injection, which were analyzed by a modified version of Cortical Box, namely, “Medial Box” method (see below for more details). What we observed in Fig. 3 was generally applicable to all these data: the strong tracer signals were generally observed as dissociated spots in layer 1 maps, but were continuous in layer 6, suggesting that axons extended

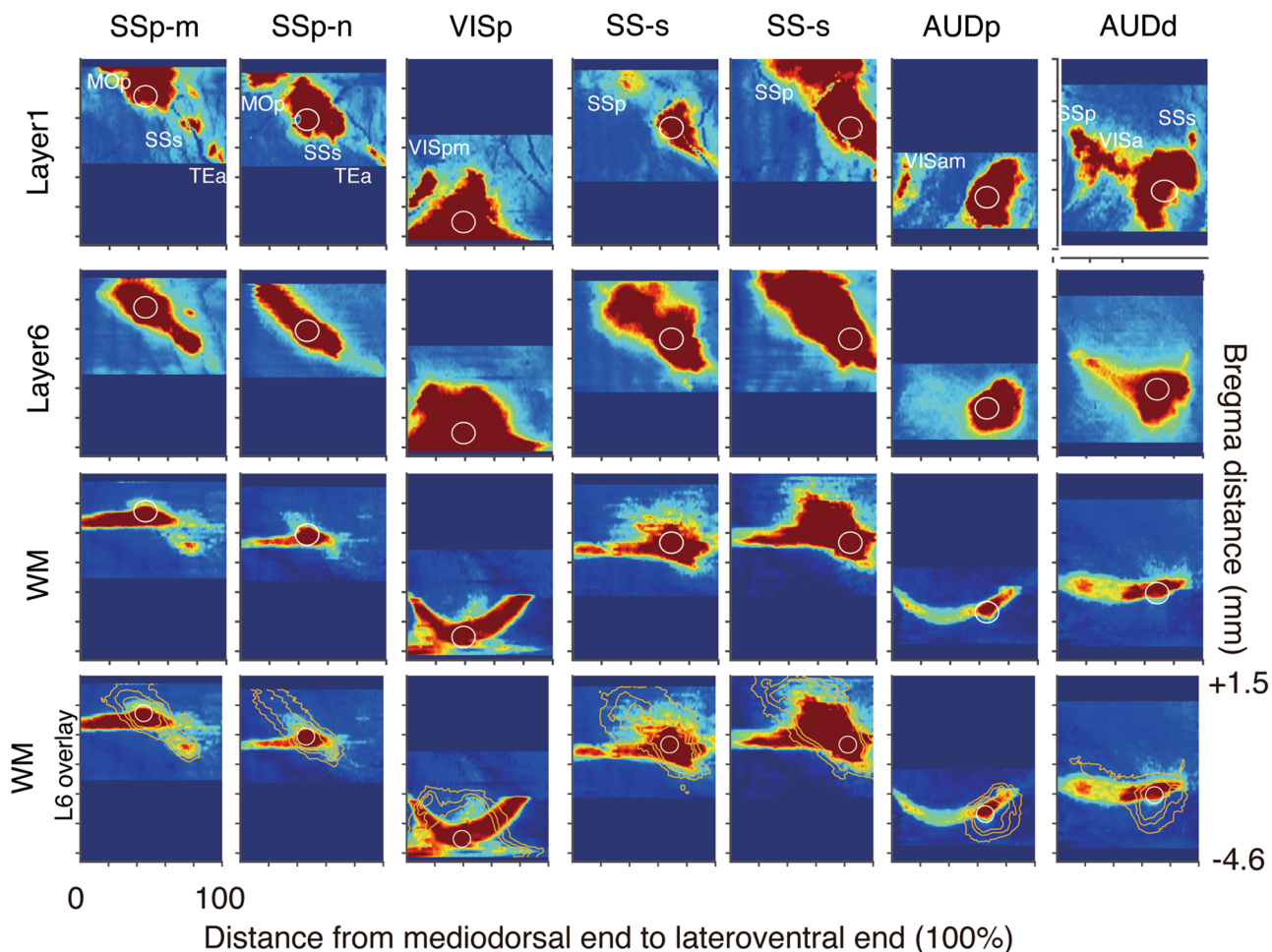


Fig. 5 Spatial distribution of axonal innervation in standardized cortical flatmaps (2). Standardized layer flatmaps for 6 different AAV tracer injections. The conventions used in this figure are the same as those in with Fig. 5

in layer 6 to reach remote targets. Strong white matter signals corresponded to those that targeted corpus callosum and internal capsule, which ran parallel to the coronal sections (appears horizontal in the flatmap). Layer 6 signals spread oblique to such horizontal lines and the overlay of the two flatmaps exhibited little overlap except around the injection site (bottom panels in Figs. 4, 5, 6, 7), showing lack of axon fibers spreading through the white matter.

In two cases of MOs injection examined by Medial box representation, we observed posterolateral cortical paths within layer 6 that continued even out of the medial box (Fig. 6f). The distinction between the gray and white matter was quite clear in the original coronal images, in which shadows of neuronal cells were identified (Fig. 6b–e). We obtained similar results for both MOs injections, although the appearance of layer 1 flatmaps was different due to different levels of signal saturation (compare Fig. 6b, c). In the case of RSA injection, the lateral spread of tracers into VISa coincided with the extension of white matter fiber that

targets the internal capsule, which we observed to send collateral toward VISa (Fig. 21). As far as we examined, this was the only clear case of white matter route innervation. To conclude, flatmap analyses demonstrated the predominance of “gray matter route” over “white matter route” for cortical projections.

Front views of Cortical Box reveal layer-specific axonal projections

To explore the laminar spread of axonal signals in more detail, we next examined the maximum intensity projection (MIP) images for frontal views of each cortical box. Figure 7 shows five such examples (the front view MIPs for all the 17 Cortical Boxes are shown in Online Resource 1). First, we show the identification of the injection centers. Although the GFP signals are saturated in green channel, we found that we can distinguish individual cell bodies from axons and/or dendrites if we examine the blue channel (Online Resource

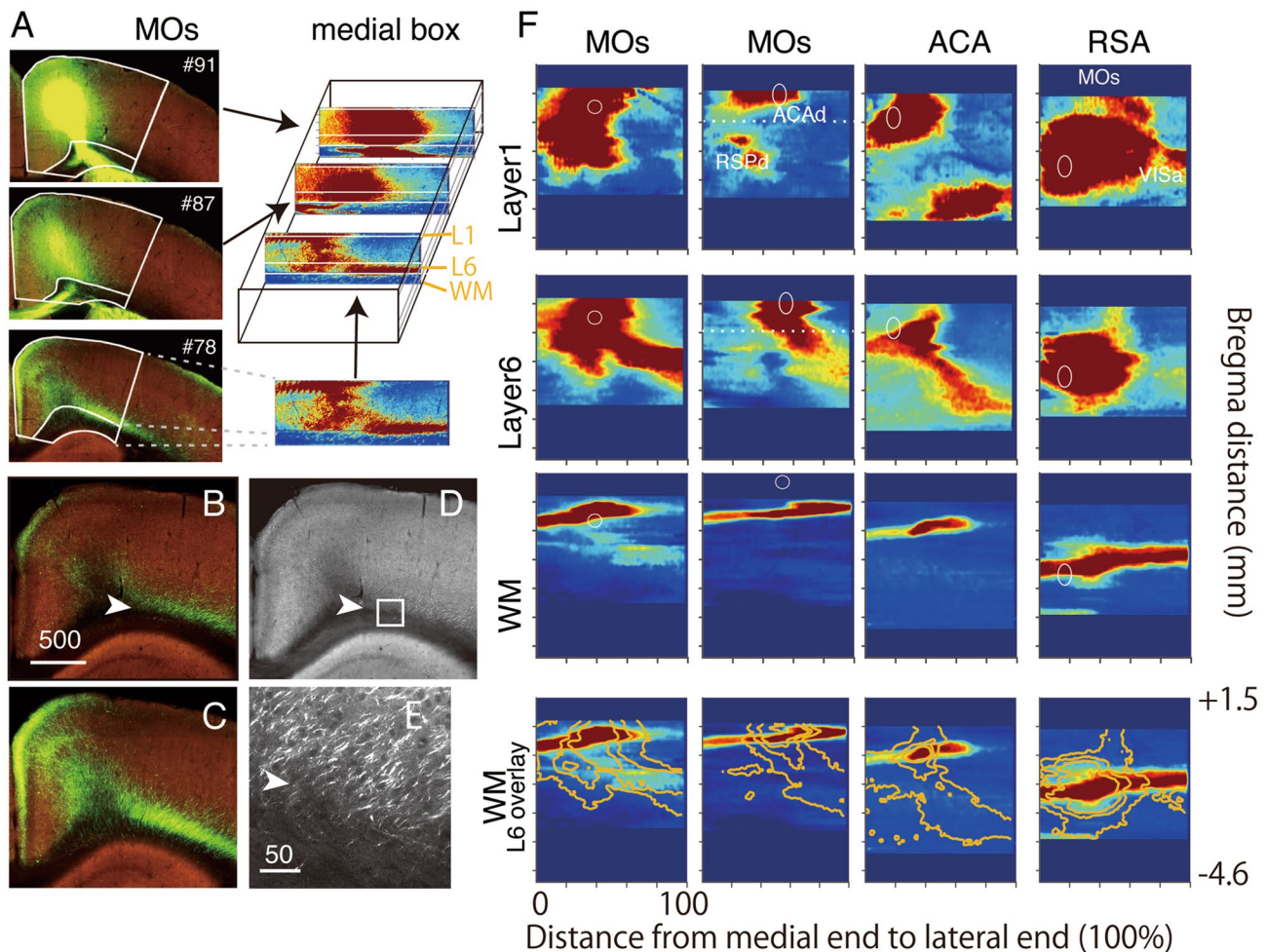


Fig. 6 Analysis of axonal projections around the medial wall. **a** The schematic view of Medial Box method, which is modified from the standard Cortical Box method. Example of cortical sections of injection into MOs (Allen data ID: 180916954). The medial end, lateral end, inner contour, and outer contour were manually determined to select the part of the cortex for further processing. The selected cortical region was converted into a standard rectangle. The same procedure was repeated for a set of coronal sections to reconstruct 3D image of the cortex. **b–e** Examples of original fluorescent images of MOs injections to show the absence of the white matter route

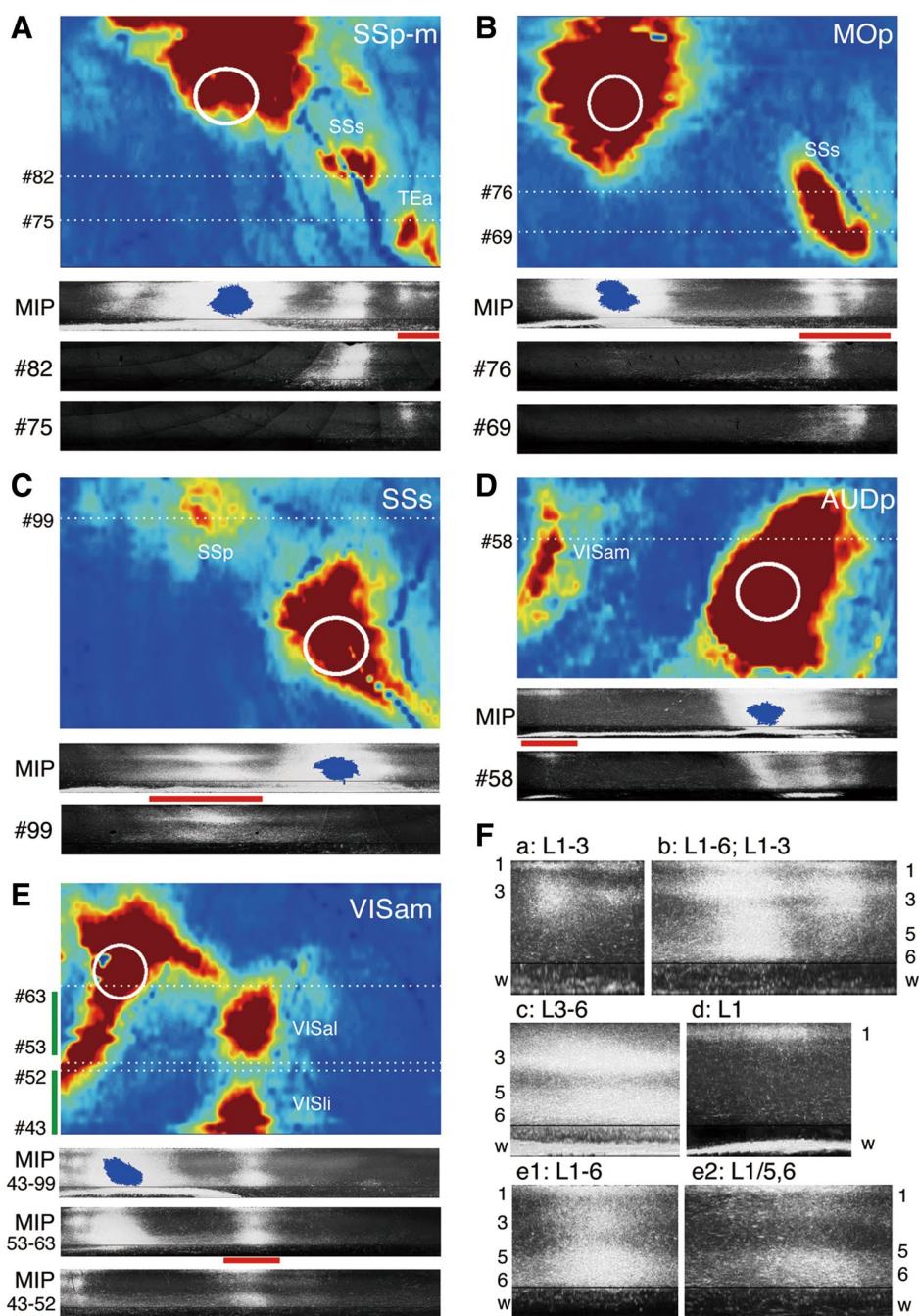
for axonal spread to the posterolateral direction. **b, c** The images of similar AP position taken from Allen Data ID 141603190 and 180916954, respectively. **d** The red channel view of **b**, which is magnified in **e** (square box). The border between layer 6 and the white matter (arrowhead) can be unambiguously identified by the presence of cell shadows in layer 6. Note that the intense axonal signals are clearly within layer 6. Scale Bars for **b–d**; 500 μm , for **e**; 50 μm . **f** Standardized layer flatmaps for six different AAV tracer injections. Same convention as in Figs. 5 and 6

4). As shown by blue shades, the injection centers thus identified are pretty well restricted and all the other saturated signals represent nearby projections. Generally speaking, such nearby signals spanned all layers and formed a large island in layer 1 flatmap. As we have seen in Figs. 4 and 5, long-range connections can be observed to occur from such an island to a discrete spot, indicating a specific point-to-point connection. In the front view MIPs, such spots were connected to the injection site through axonal signals that are mostly confined to layer 6, which is best exemplified in Fig. 6b (for MOp projection). In combination with the flatmaps shown in Figs. 3, 4 and 5, this data demonstrated high specificity of axonal spread within layer 6 for long-range

projections. In AUDp injection (Fig. 7D), however, we could not observe clear axonal pathway in the front view MIP. In this case, thin axon fibers were found dispersed in the cortical gray matter in the original high-resolution images. This example suggests that area-to-area connections can be also conveyed through dispersed axons within the gray matter.

Finally, we examined the laminar specificity of axon terminal convergence in the remote areas (Fig. 7-1F). In some cases, we observed concentration of tracer signals in layer 6, which is continuous from the “pathway signals” and accompanied concentration of tracer signals in the upper layers as well (Fig. 7-1F; b, c, e1, e2). In other examples, we observed the concentration of tracer signals in the upper layers with only

Fig. 7 Front views of Cortical Box reveal layer-specific axonal projections. Maximum Intensity Projections (MIP) for the front view of the Cortical Box visualizes the axonal projections that encompass multiple sections. **A–E** Standardized flatmaps for layer 1 of SSp-m, MOp, SSs, AUDp and VISam injections are shown together with the MIP of front views. The standardized rectangle generated from coronal section images of the original Allen atlas are also indicated with the section numbers. The injection centers determined by the cell body signals in the blue channel are shown in blue for MIP front views. The red bar below the MIP views are magnified in **F**. For **E**, the MIPs for all the analyzed sections (43–99) are shown together with the MIPs for a part of the data (53–63, 43–52). **F** The MIP front views shown by red bar in **A–E** are magnified to show different laminar patterns of terminal extensions at remote areas



passing fibers in layers 5 and 6 (Fig. 7-1F; a, b, d). Innervation in layer 1 was almost always observed, but in one case, we observed no innervation in layer 1 with concentrated tracer signals in layers 3/4 and 5/6 (Fig. 7-1F; c). These examples illustrate the variability of axonal terminations in various cortical projections.

Quantitative analyses of layer-specific cortical projection patterns

Faced with the complexity of axonal distribution patterns, we felt the need to analyze it more systematically and objectively. For this purpose, we first decomposed the Cortical

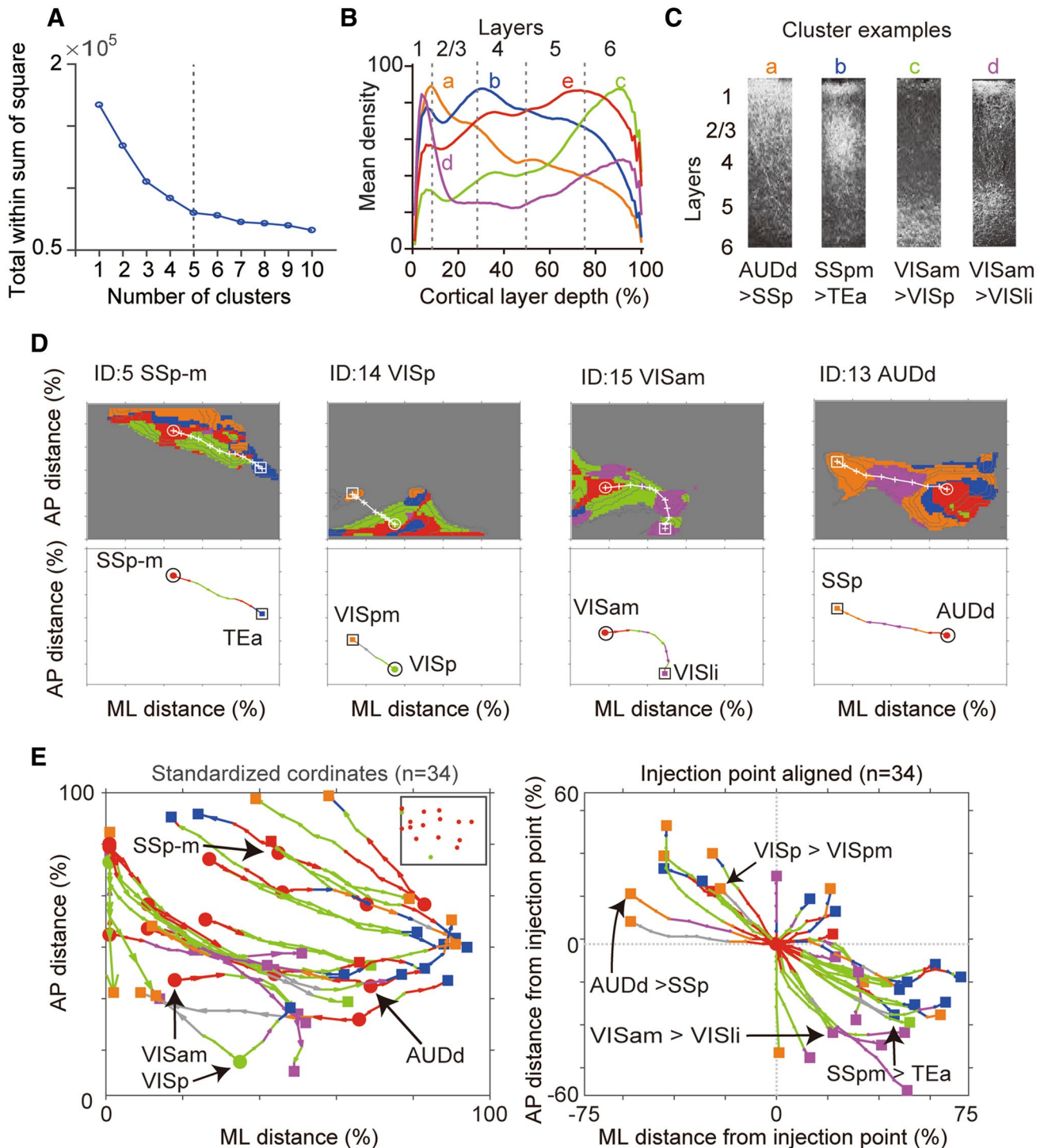


Fig. 8 Clustering analysis of layer distributions. **A** Clustering analysis for all columns of the cortical box from 17 injection samples. Similarities of clusters plotted as a function of cluster numbers used for the clustering analysis (see “Materials and methods”). **B** The averaged layer distributions of 5 clusters (patterns “a–e”) from the pial surface (0% of cortical depth) to the cortex/white matter border (100%). Approximate layer borders were noted by vertical dotted lines (0–10% for layer 1; 10–30% for layer 2/3; 30–50% for layer 4; 50–75% for layer 5; 75–100% for layer 6) following our previous studies (see “Materials and methods”). **C** Examples of actual layer pattern for each cluster. **D** Examples of cluster assignment in horizon-

tal layer map. The colors of the areas correspond to the cluster identity shown in **B**. A white circle and a rectangle in each map represent the tracer injection site and the furthest projection areas. The projection pathways connecting those two areas were indicated by white crosses and lines. The cluster identities on each projection pathway were indicated by line colors in the bottom. **E** The projection pathways (n=34) from 17 injection samples (2 pathways for each sample) were overlaid in a map (left panel). The inset indicates the 17 injection sites. The each projection pathway was aligned so that the injection point comes to the center of the figure (right panel)

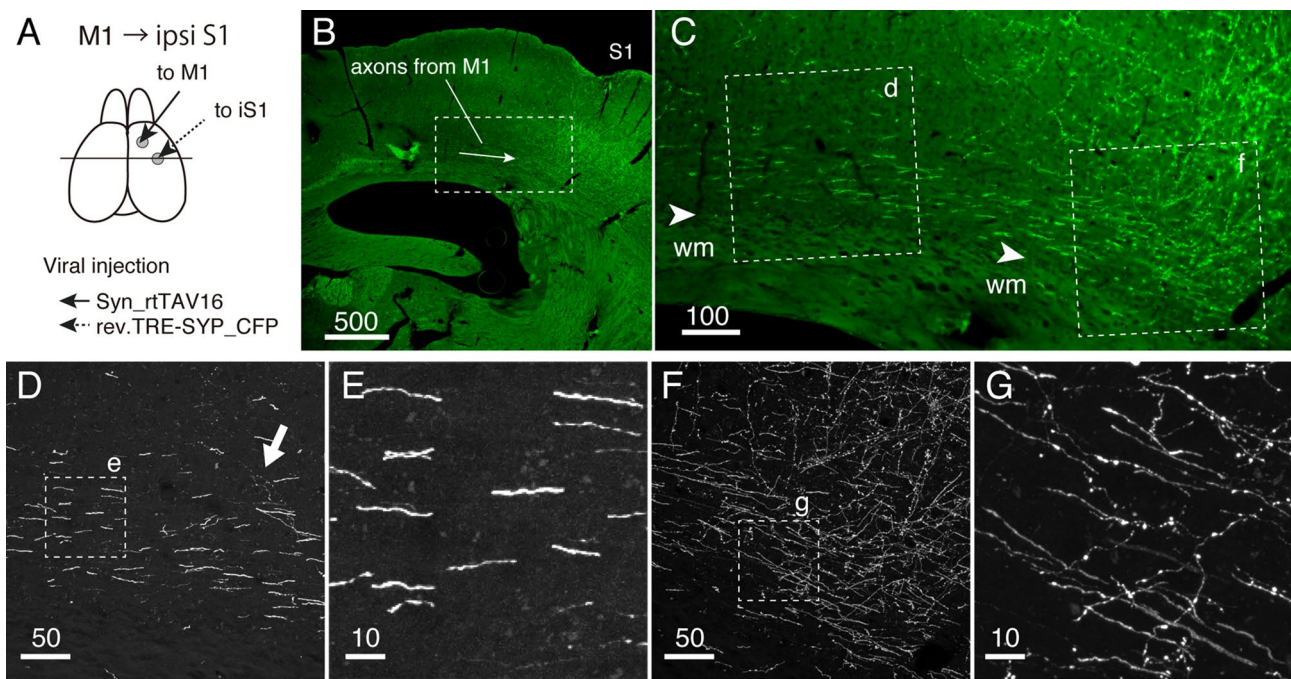


Fig. 9 Confocal imaging of the cortico-cortical axon fibers. The cortico-cortical axons that project from the motor cortex (M1) to the ipsilateral somatosensory cortex (ipsiS1) were selectively labeled for confocal imaging. **A** Schematic representation of the labeling strategy. Simultaneous injections of the NeuRet vector coding TRE-SYP_CFP into ipsiS1 and AAV coding Syn_rtTAV16 resulted in labeling of all types of connections between the two areas. **B** Low magnification view of the section immunostained by GFP antibody showing labeled axons from M1 (shown by an arrow). The rectangle region is magnified in **C**. Bar 500 μm . **C** Higher magnification view of M1-to-S1 axons. Note that the border between Layer 6 and the white mat-

ter (wm) can be unambiguously identified (arrowheads). Two regions shown by dotted squares with labels d and f were imaged by the confocal microscopy in **D**, **F**. Bar: 100 μm . **D** Maximum intensity projection image of thick axon fibers that reside at the very bottom of layer 6 in **C**. The white arrow indicates the intermingling of thin axon fibers with bouton-like varicosities. Bar: 50 μm . **E** Magnified view of **D**. Note the lack of side branches or boutons. Bar 10 μm . **F** Maximum intensity projection image of terminal arborization at ipsiS1. Note numerous fine branches to come out of layer 6 toward upper layers. Bar 50 μm . **G** Magnified view of panel F. Note the presence of bouton-like varicosities. Bar 10 μm

Box into 61×100 (APxML) arbitrary columnar modules and determined the lamina profile of each module for clustering analysis. All the cortical box data for seventeen injection samples were combined for the analysis to define common patterns of tracer distribution across datasets. Figure 8A indicates the reduction of the total within the sum of the square as the number of clusters increase, suggesting that modules with similar lamina profiles are being grouped together by clustering. Based on systematic changing of the number of clusters, we concluded that five clusters is appropriate as the first approximation (Fig. 8A, see “Materials and methods”). Figure 8B shows laminar patterns of the resulting 5 clusters. Among them, the pattern “e” represents all-layer pattern, which is often found in the vicinity of injection centers. Patterns “a–d” exhibited more or less layer specific patterns (Fig. 8B). Pattern “a” is characterized by conspicuous labeling in layer 1 with gradually decreasing signals as the layer goes deeper. Pattern “b” is similar to pattern “e”, but has characteristically enriched signals in the middle layer (2/3–4) and lack of signals at the very bottom. Pattern “c” shows signal enrichment in layer 6 with

lower signals in upper layers, whereas pattern “d” exhibited bilaminar distribution in layers 1 and deep layers with low signals in layers 2–5a. As the actual example columns show, these clusters pretty well captured the characteristic lamina patterns (Fig. 8C). One important question to be asked is the robustness of this classification. To test this, we performed the clustering using only a subset of the 17 injections and compared the obtained patterns with the original one. As shown in Online Resource 3, significant similarity to the original ($N=17$) patterns were observed only using two samples ($N=2$) for clustering and the correlation coefficient reached a high value (>0.9) when six datasets were used. Because some of the dataset had tracer spreads to more than one area, we tested the clustering with only pure injections and still we had similar result (data not shown). This result suggests that the five patterns shown in Fig. 8B is quite robust, and that comparable layer patterns can be still obtained, independent of dataset selection (Online Resource 3).

Next, we asked how these columnar modules are spatially distributed in the Cortical Boxes. To visualize it, we

color-coded the 61×100 modules for the above five patterns on each flatmap (Fig. 8D, Online Resource 2). We also overlaid the maximum intensity projection of all layers as contours (Online Resource 2). This information provided an important clue as to the approximate pathways of the axonal projections from the injection center to the peripheral targets. That is, the targets of axonal projections can be identified by the peaks of the tracer signals at the periphery because that is where the once-spread axon fibers converge and arborize to make synapses. We can also determine the most probable pathway for such projections by tracking the local maximum (white lines in Fig. 8D). Figure 8D demonstrates four of such examples (see Online Resource 2 for other examples). We selected two farthest target areas for each sample and performed this pathway analysis for all the injections. The obtained pathway information was then mapped onto a common coordinate space (Fig. 8E). By excluding nearby projections, which may contain passing fibers, we were able to simplify and more effectively capture the properties of the long-range projections out of diverse and complex axonal spreads.

Typically, pattern “e” (red) was found near the injection site, which is explained by axon fibers extending laterally from layers 2–6. Another prevalent feature was the presence of pattern “c” (green) in the middle of the pathways. This observation objectively shows that remote targets are connected by axon fibers passing through layer 6. In the case of AUDd (Fig. 8D), pattern “d” (purple) was present in place of pattern “c”, but this pattern also shows higher signals in layer 6. Regarding the topology of projections, Fig. 8E (left panel) showed that most of the long-range projections run along the anteromedial to posterolateral axis. This bias was captured more clearly by replotting the projections so that the injection site comes at the center of the plot (Fig. 8E, right panel, $p = 0.001$, Kuiper test): whereas 14 and 13 projections were found within the anteromedial and posterolateral quadrants, respectively, only seven projections were found within the anterolateral quadrant. No projection was found in posteromedial quadrant. This bias cannot be attributed to the locations of the injection sites, because they are randomly scattered (Fig. 8E, inset in left panel). Interestingly, we found that the laminar profiles at the target sites are biased depending on the direction of projections; pattern “a” was more prevalent in the anteromedial quadrant, whereas patterns “b” and “d” were more prevalent in the postero-caudal quadrant.

In previous studies, Burkhalter and coworkers proposed that the axonal targeting of layers 2–4, and of layer 1 represent feedforward and feedback projections, respectively, based on the anterograde tracing of the rodent visual areas (Coogan and Burkhalter 1993; D’Souza et al. 2016; D’Souza and Burkhalter 2017). We were interested in whether the same concept can be applied beyond the visual areas. In

our clustering scheme, pattern “d” represented enrichment in layer 1 and layer 6, pattern “a” represented enrichment in upper layers with the peak in layer 1 and pattern “b” represented enrichment in layers 2–4 with some contribution from layer 1. Therefore, the “a” and “d” patterns are considered to be “feedback”, whereas “b” pattern is considered to be “feedforward”, according to this scheme. As shown in Table 2, the projections originating from the primary areas tended to terminate with pattern “b” (12/18; 66.7%), whereas the projections originating from the higher order areas tended to terminate with patterns “a” or “d” (14/16; 87.5%). The statistical significance of this difference was confirmed by bootstrap method ($p < 0.00005$; see “Materials and methods”). This difference was observed with or without the inclusion of two datasets that infected both the primary and higher-order areas (AUDp and VISp, data not shown). We also examined the occurrence probabilities of the four lamina patterns (except pattern “e”) for the entire cortex in each injection and compared between the primary areas and higher-order areas (Online Resource 3). Note that this includes both passing fibers and terminal arbors, unlike the analysis in Table 2. In both categories, pattern “c” was high, which is considered to be axon pathway. We observed statistical difference in patterns “b” and “d”, which were more abundant in the primary ($p < 0.05$) and higher order areas ($p < 0.005$), respectively. The differential occurrence probability of pattern “d”, which represents enrichment in layers 1 and 6, was especially striking. This is interesting, because the “feedback” projection of macaque visual cortices also targets layers 1 and 6 (Rockland and Pandya 1979; Felleman and Van Essen 1991). Thus, our data appear to suggest the existence of similar rule for area-specific innervation patterns between mouse and primates.

Fine morphological analyses of axonal fibers that project from M1 to the ipsilateral S1

The prevalence of layer 6 pathways for cortical projections let us wonder whether the axon fibers in layer 6 form synapses on the way to the remote targets. Although the axon fibers that populated in layer 6 appeared to be thick with no boutons (e.g., see Fig. 1c), the Allen Connectivity atlas lacked the resolution to examine this point with confidence. So, we examined our own injection sample by confocal microscopy with higher resolution (Watakabe et al. 2014). As shown in Fig. 9A, retrograde lentiviral vectors harboring fluorescent marker protein (SYP-CFP) under the TRE promoter was injected in S1, whereas TET activator in AAV was injected in M1 (Fig. 9A). Ideally, all kinds of neurons that link M1 and S1 are labeled by co-infection (Fig. 9B–G). In the Allen two-photon image data, the myelinated white matter region appeared dark and the true border between the cell-rich gray matter and cell-sparse white matter was

not necessarily clear (see legend for Fig. 1). The low-magnification fluorescent microscope image of our sample was better in this respect, clearly visualizing the white/gray matter border by different tissue autofluorescence texture (Fig. 9C, arrowhead). It is obvious that the axonal fibers that connect M1 and S1 were entirely contained within the gray matter (Fig. 9C). At this low magnification, we were able to observe the axon fibers within layer 6 (Fig. 9C, D) to branch into small fibers that run perpendicular toward the surface (Fig. 9C, E). The confocal microscopic analysis further showed qualitative differences in the morphology of axon fibers that populate the route and terminals of these axon fibers. In the terminal region (S1), the axon fibers were thin and formed bouton-like varicosities (Fig. 9C, F, G). In contrast, we observed relatively thick axon fibers with few axon branches, if any, that lacked varicosities within the layer 6 route (Fig. 9D, E). Since we could observe fine fibers with varicosities to coexist with such thick fibers, there may exist some synaptic connections during the layer 6 pathway. Nevertheless, the majority of the axon fibers in layer 6, in this case, appeared to represent passing fibers without synaptic connections. Although this data alone is insufficient to conclude that the layer 6 axon fibers generally lack en passant synapses, it demonstrated the existence of passing fibers with few or no synapses on the route to the target even within the gray matter.

Discussion

The main finding of the current study is the predominance of the “gray matter route” over the “white matter route” for ipsilateral cortico-cortical connectivity in the mouse brain. To our knowledge, this point has never been investigated in a systematic way. In our study, we inspected the projection patterns of 23 different injections and analyzed in depth the 17 injections of the dorsolateral regions by Cortical Box method. With exception of RSA (Fig. 2I) and medial and orbital frontal cortices (Online Resource 5), the majority of the ipsilateral projections proceeded through the gray matter, whereas the contralateral projections proceeded through the white matter (e.g., see Online Resource 5, panel A4). Detailed laminar analyses revealed a complex architecture of the mouse projections within the gray matter. In the vicinity of the injection sites, we observed horizontal extension of the axon fibers in both upper and lower layers, which is similar to the primate intrinsic connections (Levitt et al. 1993; Lund et al. 1993). On the other hand, we also found point-to-point connectivity for long-range connections, which appeared as a discrete spot in the upper layer flatmap. The majority of such spots were connected via axons in layer 6, which is reminiscent of the primate’s extrinsic connections traveling through the white matter. The confocal microscopic

analysis raised a possibility that these layer 6 axon fibers may include passing fibers with no synaptic connections. Interestingly, the projections from the primary and higher-order areas to the distant targets preferentially terminated in layers 2–4 and layer 1, respectively, suggesting possible hierarchical organization similar to that of macaques (Rockland and Pandya 1979; Felleman and Van Essen 1991; Coogan and Burkhalter 1993; D’Souza et al. 2016; D’Souza and Burkhalter 2017). Overall, our study showed differences and similarities of the cortico-cortical connectivity in the mouse and primate brains, which will be useful in extrapolating the mouse study to humans.

Technical considerations

Although Allen Mouse Brain Connectivity atlas provided excellent data for the investigation of the mouse connectivity, several complications need to be cautioned. First, as is generally true with any anterograde tracers, the AAV tracer has a problem of retrograde infection (Oh et al. 2014) and/or anterograde transsynaptic infection (Zingg et al. 2014). The visual inspection of the original image data, indeed, found labeling of the cell bodies in the terminal regions, although axonal extension from such labeled cells appeared to be relatively weak. Second, the dataset we used included injections that spread to more than one area (Table 1). Such mixed injection can potentially have a serious effect on analyzing the network structure as discussed in a recent study (Gămănuț et al. 2018). This, however, did not affect our analysis so much, because we were only comparing “primary” versus “higher” areas, which were mostly well segregated (see Table 1). Third, the resolution of the image dataset of the Allen atlas was not high enough to clearly identify boutons. As we have shown in Fig. 9, AAV tracers label both passing and synapsing fibers, which cannot be correctly distinguished in the Allen dataset. It is, therefore, necessary to keep in mind that the tracer signal strength is not equal to connection strength. Having said this, we believe that there is certain correlation between them, especially at the peripheral regions, where the synapsing fibers arborize to make synapses. Fourth, the tracer signals of the database tended to be weaker in the white matter region, probably due to optical interference of highly myelinated tissue. Regarding this point, we believe that the effect was minimal because we could detect even thin corticostriatal fibers within the white matter. Finally, many of the lateral AAV injections were restricted to the lower layers, and we could not always select injections that cover the entire layers for the wild-type samples (e.g., see Fig. 7). This is probably because of limited dispersion of AAV by the iontophoretic injection (Oh et al. 2014). We did not pursue this problem further, because we could not find appropriate datasets to estimate this influence.

More detailed studies using layer-specific transgenic lines may, in the future, solve this problem.

Cortical Box method was previously developed to standardize and quantify histological serial section data (Hirokawa et al. 2008a, b; Watakabe et al. 2012). With a modification to distinguish the white and gray matter compartment, it proved to be a powerful tool to visualize and analyze the cortical axonal projections. The clustering analysis, in particular, provided an objective means to investigate the layer-specific axonal extensions. One pitfall of the current analysis is that the tracer signals are often saturated near the injection site and at some terminal regions. When the tracer signals are saturated, it affects the relative abundance even after normalization (e.g., see Fig. 6). This is a difficult problem to overcome because it requires the improvement in various steps of labeling and imaging. Nevertheless, we believe that the effect of saturation is kept minimal thanks to systematic experimental design of the Allen dataset.

Evolutionary consideration of inter-area wiring

The wiring of larger brains poses a serious issue, with many more neurons to communicate and at longer distance (Ringo 1991; Kaas 2000; Hofman 2014). On top of this, larger brains are equipped with myelinated large-caliber axon fibers to achieve fast axonal conductance for synchronizing distant brain regions (Wang et al. 2008; Buzsáki et al. 2013; Liewald et al. 2014). As a result, the white matter volume is disproportionately greater in a large brain and it amounts to almost the same size as the gray matter in humans (Pakkenberg and Gundersen 1997). It is quite possible that the cortical fibers segregated into the white matter as an evolutionary adaptation to allow more space for intra-cortical circuits and led to modularization of individual cortical areas. Such modularization may have been critical for achieving higher level of functional specialization and its integration in primates.

The comparative studies of the cortical size suggests that the expansion of the gray and white matters occurred in synchrony: a universal scaling law can account for the relative ratio of the gray and white matter of the cerebral cortex across 59 species over size difference of five to six orders of magnitude (Zhang and Sejnowski 2000). This rule is applicable to both rodents (including mice and rats) and primates, despite different routing of the ipsilateral cortical connections. In a theoretical study to explain this law, it was postulated that the unit cortical area sends and receives the same amount of inter-areal white matter fibers across species (Zhang and Sejnowski 2000). According to our finding, the white matter consists mostly of callosal and subcortical projection fibers in mice, whereas the ipsilateral cortical fibers should occupy a large space in primates with larger brains. To understand the evolutionary constraints of the cerebral cortex, it would become necessary to re-estimate

the constituents of the white matter into callosal, extrinsic ipsilateral cortical and subcortical projections and clarify the rodent/primate difference as well as common constraints across species.

It was proposed that connective properties of the brain network can be understood as a “small-world” type design, in which locally connected regions serve as “hubs” to achieve overall well-connected network structure (Bullmore and Sporns 2009, 2012; Goulas et al. 2017). Recent high-quality tracing data, however, revealed that the cortical network consists of high density graphs with weight heterogeneity, rather than a sparse binary connections that was initially postulated, leading to a new theoretical framework to cope with such data (Markov et al. 2011, 2014a, 2014b; Wang et al. 2012; Ercsey-Ravasz et al. 2013; Bassett and Bullmore 2016; Horvát et al. 2016; Gămănuț et al. 2018). A cardinal feature found through analyses of the macaque retrograde tracing data was the correlation of connection weight and distance, which was called as exponential distance rule or EDR (Ercsey-Ravasz et al. 2013). It was later found that this rule also applies to mice (Horvát et al. 2016). Thus, although the main routes of ipsilateral cortical connections are different in mice and macaques, similar network rules appear to apply for both species.

Areal and laminar organization of mouse cortical projections

Taking advantage of the rich dataset, we selected representative areas for cortical projections and performed objective analyses of areal and laminar cortical projections by Cortical Box method. By focusing on long-range projections, we were able to simplify the complex distribution of axonal signals. One of the most striking features of the areal distribution was the bias of long-range connections in the antero-medial–posterolateral (AM/PL) direction. According to the laminar profiling, these connections often pass through the layer 6 route (Fig. 8E), which may consist of non-branching and thick connection fibers (Fig. 9). These observations suggest tight coupling of cortical areas in AM-PL positions but not across. Similar topological connectivity is previously suggested in viral tracer mapping (see Fig. 4 of Zhang et al. 2016). Consistent with the structural mapping, synchronization of calcium activity is observed in a similar direction in a resting-state imaging of GCaMP6f-expressing transgenic mice (Vanni et al. 2017), or in resting state fMRI imaging (Liska et al. 2015). These studies support the idea that the AM/PL bias of connection is functionally meaningful.

It is also noteworthy that we observed “direction-specific” laminar targeting in long-range connections. As shown in Fig. 8E, the terminal laminar profiles exhibited differential patterns depending on the direction of projections (antero-medial or posterolateral). We suspect that this may reflect

relative positioning of primary and higher-order areas. The concept of hierarchical organization of the cortical areas was originally formulated based on segregated laminar targeting of visual area connectivity in the macaque monkey and was later extended to the entire cortical areas (Rockland and Pandya 1979; Felleman and Van Essen 1991). This influential concept was, nevertheless, not easily transferable to the rodent cortex. Whereas Burkhalter and coworkers showed the existence of many “higher” visual areas (Coogan and Burkhalter 1993; Wang and Burkhalter 2007; Wang et al. 2012), the input layer specificity and/or inter-area connectivities were somewhat different between rodents and primates (reviewed in D’Souza and Burkhalter 2017). They suggested that the ratio of layer 2–4 and layer 1 inputs as the conserved metric of cortical hierarchy and used it to demonstrate the hierarchical order of the visual areas (Coogan and Burkhalter 1993; D’Souza et al. 2016; D’Souza and Burkhalter 2017). With similar criteria for analysis, we found evidence that the hierarchically “low (primary)” and “high” areas exhibit differential preferences for lamina targeting (Table 2). In this analysis, we focused only on long-range terminal connections, which are supposed to have small contribution of passing fibers. Because such long-range connections often crossed modality in mice (e.g., MOp to SS-s), we infer that the hierarchical or directional connectivity likely exists beyond modality. From the functional point of view, the inputs to layer 1 and deep layers, which correspond to “feedback” input layers, are suggested to have profound effects on somatosensory (Manita et al. 2015) and visual (Leinweber et al. 2017) sensations beyond simple modulatory effects. The generality of this finding is a matter of future study. It should also be important to determine the contributions of different cortical cell types for feedforward and feedback projections. Future use of layer-specific transgenic lines would become necessary to clarify this point.

References

- Bassett DS, Bullmore ET (2016) Small-world brain networks revisited. *Neuroscientist* 23:499–516
- Bullmore E, Sporns O (2009) Complex brain networks: graph theoretical analysis of structural and functional systems. *Nat Rev Neurosci* 10:186–198
- Bullmore E, Sporns O (2012) The economy of brain network organization. *Nat Rev Neurosci* 13:336–349
- Buzsáki G, Logothetis N, Singer W (2013) Scaling brain size, keeping timing: evolutionary preservation of brain rhythms. *Neuron* 80:751–764
- Coogan TA, Burkhalter A (1993) Hierarchical organization of areas in rat visual cortex. *J Neurosci* 13:3749–3772
- D’Souza RD, Burkhalter A (2017) A laminar organization for selective cortico-cortical communication. *Front Neuroanat* 11:71
- D’Souza RD, Meier AM, Bista P, Wang Q, Burkhalter A (2016) Recruitment of inhibition and excitation across mouse visual cortex depends on the hierarchy of interconnecting areas. *Elife* 5:e19332
- Ercsey-Ravasz M, Markov NT, Lamy C, Van Essen DC, Knoblauch K, Toroczkai Z, Kennedy H (2013) A predictive network model of cerebral cortical connectivity based on a distance rule. *Neuron* 80:184–197
- Felleman DJ, Van Essen DC (1991) Distributed hierarchical processing in the primate cerebral cortex. *Cereb Cortex* 1:1–47
- Finlay BL (2016) Principles of network architecture emerging from comparisons of the cerebral cortex in large and small brains. *PLoS Biol* 14:e1002556
- Gămănuț R, Kennedy H, Toroczkai Z, Ercsey-Ravasz M, Van Essen DC, Knoblauch K, Burkhalter A (2018) The mouse cortical connectome, characterized by an ultra-dense cortical graph, maintains specificity by distinct connectivity profiles. *Neuron* 97:698–715.e10
- Goulas A, Uylings HBM, Hilgetag CC (2017) Principles of ipsilateral and contralateral cortico-cortical connectivity in the mouse. *Brain Struct Funct* 222:1281–1295
- Hirokawa J, Bosch M, Sakata S, Sakurai Y, Yamamori T (2008a) Functional role of the secondary visual cortex in multisensory facilitation in rats. *Neuroscience* 153:1402–1417
- Hirokawa J, Watakabe A, Ohsawa S, Yamamori T (2008b) Analysis of area-specific expression patterns of RORbeta, ER81 and Nurr1 mRNAs in rat neocortex by double in situ hybridization and cortical box method. *PLoS One* 3:e3266
- Hofman MA (2014) Evolution of the human brain: when bigger is better. *Front Neuroanat* 8:15
- Horvát S, Gămănuț R, Ercsey-Ravasz M, Magrou L, GăăuțB, Van Essen DC, Burkhalter A, Knoblauch K, Toroczkai Z, Kennedy H (2016) Spatial embedding and wiring cost constrain the functional layout of the cortical network of rodents and primates. *PLoS Biol* 14:e1002512
- Kaas JH (2000) Why is brain size so important: design problems and solutions as neocortex gets bigger or smaller. *Brain Mind* 1:7–23
- Leinweber M, Ward DR, Sobczak JM, Attinger A, Keller GB (2017) A sensorimotor circuit in mouse cortex for visual flow predictions. *Neuron* 95:1420–1432.e5
- Levitt JB, Lewis DA, Yoshioka T, Lund JS (1993) Topography of pyramidal neuron intrinsic connections in macaque monkey prefrontal cortex (areas 9 and 46). *J Comp Neurol* 338:360–376
- Liewald D, Miller R, Logothetis N, Wagner H-J, Schüz A (2014) Distribution of axon diameters in cortical white matter: an electron-microscopic study on three human brains and a macaque. *Biol Cybern* 108:541–557
- Liska A, Galbusera A, Schwarz AJ, Gozzi A (2015) Functional connectivity hubs of the mouse brain. *Neuroimage* 115:281–291
- Lund JS, Yoshioka T, Levitt JB (1993) Comparison of intrinsic connectivity in different areas of macaque monkey cerebral cortex. *Cereb Cortex* 3:148–162
- Manita S, Suzuki T, Homma C, Matsumoto T, Odagawa M, Yamada K, Ota K, Matsubara C, Inutsuka A, Sato M, Ohkura M, Yamanaka A, Yanagawa Y, Nakai J, Hayashi Y, Larkum ME, Murayama M (2015) A top-down cortical circuit for accurate sensory perception. *Neuron* 86:1304–1316
- Markov NT, Misery P, Falchier A, Lamy C, Vezoli J, Quilodran R, Gariel MA, Giroud P, Ercsey-Ravasz M, Pilaz LJ, Huissoud C, Barone P, Dehay C, Toroczkai Z, Van Essen DC, Kennedy H, Knoblauch K (2011) Weight consistency specifies regularities of macaque cortical networks. *Cereb Cortex* 21:1254–1272
- Markov NT, Vezoli J, Chameau P, Falchier A, Quilodran R, Huissoud C, Lamy C, Misery P, Giroud P, Ullman S, Barone P, Dehay C, Knoblauch K, Kennedy H (2014a) Anatomy of hierarchy: feed-forward and feedback pathways in macaque visual cortex. *J Comp Neurol* 522:225–259

- Markov NT, Ercsey-Ravasz MM, Ribeiro Gomes AR, Lamy C, Magrou L, Vezoli J, Misery P, Falchier A, Quilodran R, Gariel MA, Sallet J, Gamanut R, Huissoud C, Clavagnier S, Giroud P, Sappey-Marinié D, Barone P, Dehay C, Toroczkai Z, Knoblauch K, Van Essen DC, Kennedy H (2014b) A weighted and directed interareal connectivity matrix for macaque cerebral cortex. *Cereb Cortex* 24(1):17–36
- Oh SW, Harris JA, Ng L, Winslow B, Cain N, Mihalas S, Wang Q, Lau C, Kuan L, Henry AM, Mortrud MT, Ouellette B, Nguyen TN, Sorensen SA, Slaughterbeck CR, Wakeman W, Li Y, Feng D, Ho A, Nicholas E, Hirokawa KE, Bohn P, Joines KM, Peng H, Hawrylycz MJ, Phillips JW, Hohmann JG, Wohnoutka P, Gerfen CR, Koch C, Bernard A, Dang C, Jones AR, Zeng H (2014) A mesoscale connectome of the mouse brain. *Nature* 508:207–214
- Pakkenberg B, Gundersen HJ (1997) Neocortical neuron number in humans: effect of sex and age. *J Comp Neurol* 384:312–320
- Paxinos G (2014) The rat nervous system, fourth edition. Academic, New York
- Paxinos G, Franklin KBJ (2004) The mouse brain in stereotaxic coordinates. Elsevier, Amsterdam
- Ragan T, Kadiri LR, Venkataraju KU, Bahlmann K, Sutin J, Taranda J, Arganda-Carreras I, Kim Y, Seung HS, Osten P (2012) Serial two-photon tomography for automated ex vivo mouse brain imaging. *Nat Methods* 9:255–258
- Ringo JL (1991) Neuronal interconnection as a function of brain size. *Brain Behav Evol* 38:1–6
- Rockland KS, Pandya DN (1979) Laminar origins and terminations of cortical connections of the occipital lobe in the rhesus monkey. *Brain Res* 179:3–20
- Schüz A, Chaimow D, Liewald D, Dortenman M (2006) Quantitative aspects of corticocortical connections: a tracer study in the mouse. *Cereb Cortex* 16:1474–1486
- Tamamaki N, Yanagawa Y, Tomioka R, Miyazaki J-I, Obata K, Kaneko T (2003) Green fluorescent protein expression and colocalization with calretinin, parvalbumin, and somatostatin in the GAD67-GFP knock-in mouse. *J Comp Neurol* 467(1):60–79
- Vanni MP, Chan AW, Balbi M, Silasi G, Murphy TH (2017) Mesoscale mapping of mouse cortex reveals frequency-dependent cycling between distinct macroscale functional modules. *J Neurosci* 37:7513–7533
- Wang Q, Burkhalter A (2007) Area map of mouse visual cortex. *J Comp Neurol* 502:339–357
- Wang SS-H, Shultz JR, Burish MJ, Harrison KH, Hof PR, Towns LC, Wagers MW, Wyatt KD (2008) Functional trade-offs in white matter axonal scaling. *J Neurosci* 28:4047–4056
- Wang Q, Sporns O, Burkhalter A (2012) Network analysis of cortico-cortical connections reveals ventral and dorsal processing streams in mouse visual cortex. *J Neurosci* 32:4386–4399
- Watakabe A, Hirokawa J, Ichinohe N, Ohsawa S, Kaneko T, Rockland KS, Yamamori T (2012) Area-specific substratification of deep layer neurons in the rat cortex. *J Comp Neurol* 520:3553–3573
- Watakabe A, Takaji M, Kato S, Kobayashi K, Mizukami H, Ozawa K, Ohsawa S, Matsui R, Watanabe D, Yamamori T (2014) Simultaneous visualization of extrinsic and intrinsic axon collaterals in Golgi-like detail for mouse corticothalamic and corticocortical cells: a double viral infection method. *Front Neural Circ* 8:110
- Zhang ZW, Deschênes M (1997) Intracortical axonal projections of lamina VI cells of the primary somatosensory cortex in the rat: a single-cell labeling study. *J Neurosci* 17:6365–6379
- Zhang K, Sejnowski TJ (2000) A universal scaling law between gray matter and white matter of cerebral cortex. *Proc Natl Acad Sci USA* 97:5621–5626
- Zhang S, Xu M, Chang W-C, Ma C, Hoang Do JP, Jeong D, Lei T, Fan JL, Dan Y (2016) Organization of long-range inputs and outputs of frontal cortex for top-down control. *Nat Neurosci* 19:1733–1742
- Zingg B, Hintiryan H, Gou L, Song MY, Bay M, Bienkowski MS, Foster NN, Yamashita S, Bowman I, Toga AW, Dong H-W (2014) Neural networks of the mouse neocortex. *Cell* 156:1096–1111